Application of azimuth moveout to the coherent partial stacking of a 3-D marine data set

Biondo Biondi, Sergey Fomel, and Nizar Chemingui[1]

ABSTRACT

The application of azimuth moveout (AMO) to a marine 3-D data set shows that by including AMO in the processing flow the high-frequency steeply-dipping energy can be better preserved during partial stacking over a range of offsets and azimuths. Since the test data set requires 3-D prestack depth migration to handle strong lateral velocity variations, the results of our tests support the applicability of AMO to prestack depth imaging problems.

INTRODUCTION

The amount of computations required by 3-D prestack depth migration is so high that its turnaround time and processing cost often discourage its usage, or, in the most of the cases, prevent from performing as many migration iterations as needed to estimate a satisfactory migration velocity model. Since the cost of migration is approximately proportional to the amount of data to be migrated, a simple and effective method to decrease the computational cost is to reduce the amount of input data. The most obvious way to accomplish this data reduction is to migrate only a subset of the available traces. To minimize the effects of data aliasing caused by the data subsampling, the input traces can be selected according to a quasi-random selection criterion (Zhou and Schuster, 1995). This method can be attractive in high signal-to-noise areas when all the data offsets are stacked during migration. However, when the signal-to-noise ratio is low, and/or when a prestack analysis of migration results is desired, either for velocity estimation or for AVO purposes, the trade-offs of neglecting available data traces should be carefully evaluated.

An alternative method for reducing the amount of data prior to migration is partial stacking of the input traces that have similar offsets and azimuths (Hanson and Witney, 1995). This method is more robust with respect to noise, either coherent or uncoherent, because it uses all the available traces to improve the signal-to-noise ratio. The more coherent the reflections are before partial stacking, the more the desired signal will be enhanced in the results. Normal moveout (NMO) increases coherency of reflections over offsets by a first-order correction of their traveltime. However, a simple trace-to-trace transformation such as NMO is insufficient when reflections have conflicting dips or in presence of diffractions. In these cases, it is

[1]**email:** biondo@sep.stanford.edu

necessary to apply to the data a partial prestack migration operator that moves energy across midpoints. In previous reports (Biondi and Chemingui, 1994; Chemingui and Biondi, 1995; Fomel and Biondi, 1995a,b) we introduced a new operator, called azimuth moveout (AMO), that transforms common-azimuth common-offset data to equivalent data at different azimuth and/or offset. AMO can be considered a generalization of dip moveout (DMO), in the sense that it transforms prestack data into equivalent data with an arbitrary offset and azimuth; in contrast DMO is only capable of transforming non zero-offset data to zero-offset data.

In this paper we present the result of applying AMO prior to partial stacking to a marine data set recorded in the North Sea. We compare the results of partial stacking after NMO and AMO with the results of partial stacking after simple NMO. The data set is a valuable test case for AMO because it shows numerous fault diffractions and because it requires 3-D prestack depth migration (Hanson and Witney, 1995) to be properly imaged. Reflections are affected by shallow velocity variations created by variable thickness in the low-velocity Tertiary sediments and in a high velocity Cretaceous Chalk layer.

To produce the results presented in this paper we used an implementation of integral AMO process based on the analysis developed in previous reports (Biondi and Chemingui, 1994; Chemingui and Biondi, 1995; Fomel and Biondi, 1995a,b). In particular, we applied the results on the operator aperture and anti-aliasing techniques presented by Fomel and Biondi (1995a; 1995b). The main technical aspects of our implementation of the AMO integral operator are summarized in Appendix A.

TEST RESULTS

The test data set that we processed was collected in the North Sea and was kindly made available to SEP by Conoco. Figure 1 shows a common-offset in-line section of the data set, at the offset of 1 km. The diffractions caused by the complex faulting, visible in the middle of the section between .8 and 1.2 seconds, are potential candidates for showing the advantages of applying AMO prior to partial stacking. These diffractions are mostly originated below the Cretaceous Chalk, and thus they travel through a fair amount of lateral velocity variations before being recorded at the surface. The brighter reflectors in the lower part of the section are generated at the salt-sediment interfaces. The fairly steep reflections at the bottom of the section are caused by the flanks of the salt swells.

The data acquisition configuration was double-source and triple streamer. The nominal common-midpoint spacing was 9.375 meters in the in-line direction, and 25 meters in the cross-line direction. The cable length was $2,200$ meters, with maximum feathering of approximately 17 degrees. To make the data handling and processing quicker, we processed only a subset of the whole data set. We windowed in time the data traces up to 512 time-samples, for a maximum time of 2.044 seconds. We selected the central 512 midpoints in the in-line direction, for a total length of $4,800$ meters, and 130 midpoints in the cross-line, for a total width of $3,250$ meters. Figure 2 shows the offset-azimuth distribution of a small subset of the data traces. As it is typical for such acquisition geometry, it shows six distinct trends, most distinguishable at small offsets, that correspond to each possible source-streamer pair.

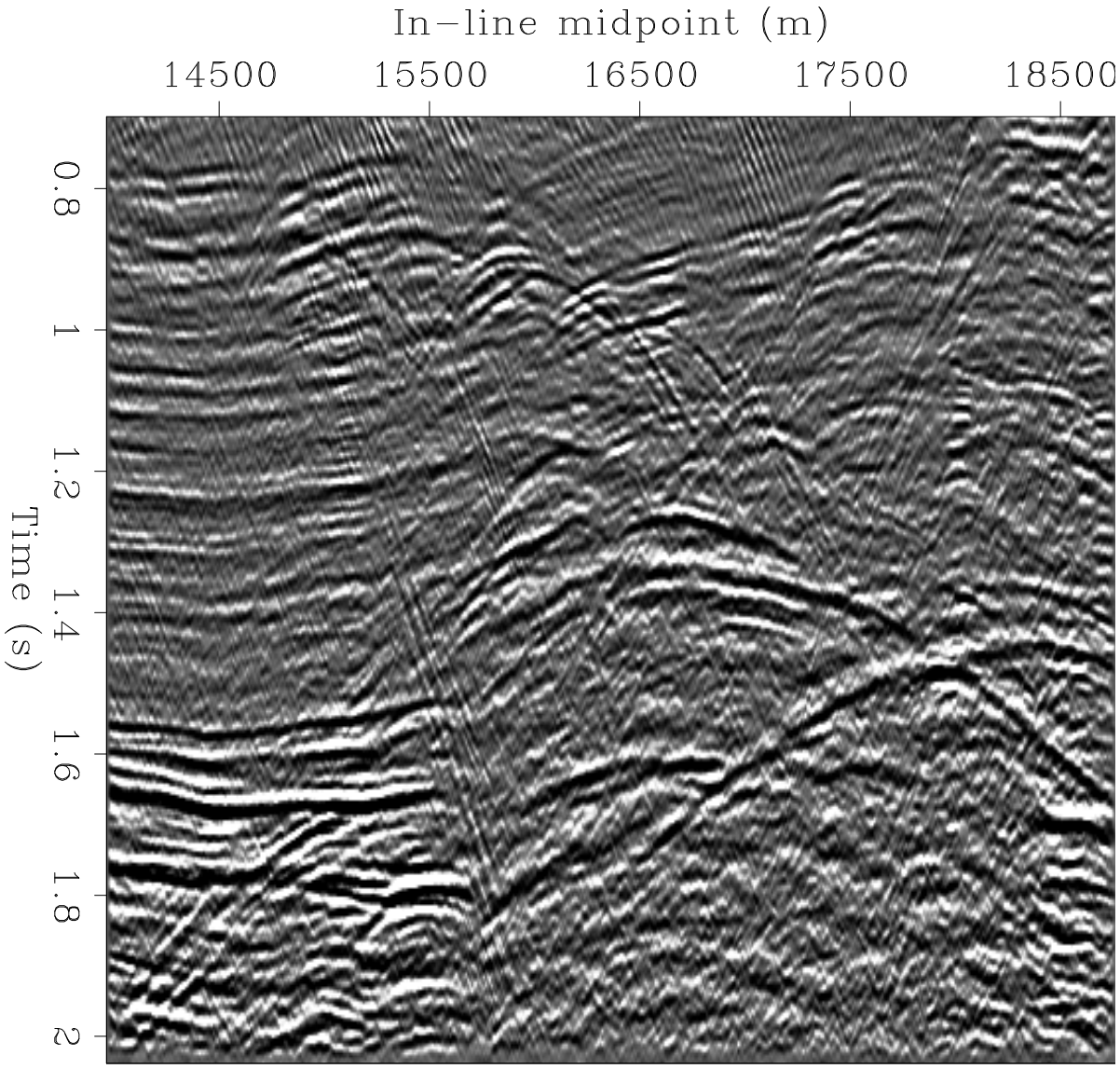

Figure 1: In-line section of the North Sea data set used for testing AMO amo3d-Over [NR]

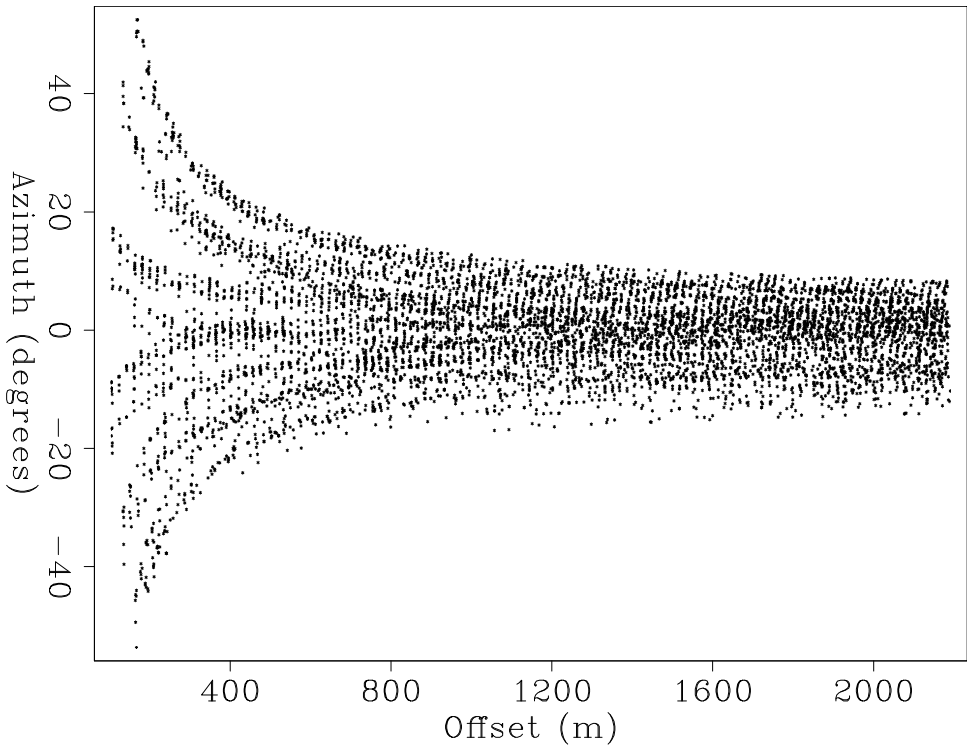

Figure 2: Offset-azimuth distribution of the test data set. amo3d-OffAzsm [NR]

We performed our test on a subset of the input traces. We selected all the traces with the offset in the range between 800 m and 1,200 meters. We applied two distinct partial stacking methods to this subset: NMO followed by binning and partial stacking and NMO followed by AMO and partial stacking. In both cases the output data were a regularly sampled cube with nominal offset of 1,000 meters and zero azimuth. To achieve as high accuracy as possible, the binning operation laterally interpolated the traces in the midpoint direction while stacking them into the output cube.

The number of input traces was about 460,000, while the output cube had 512 midpoints in the in-line direction, and 130 in the cross-line, for a total of 66,560 output traces. Therefore, the data reduction rate achieved by partial stacking is approximately 7.

Before processing the data, we applied a hyperbolic mute with a sharp cut-off. The mute velocity was slightly lower than water velocity, to assure the removal of the first arrival and some severely aliased noise at the far-offset. After muting, we applied NMO using a velocity function varying with midpoint and time. The NMO velocity function was given to us by Conoco together with the data. No inverse NMO was applied to the results before displaying, thus the reflection timings are equivalent "zero-offset" times. Of course, inverse NMO ought to be applied prior to inputting the AMO results into a prestack depth migration. Since we have not a 3-D prestack Kirchhoff depth migration program available yet, we have not completed the proposed prestack imaging flow; we plan to do that in the near future.

Figure 3 shows a comparison of the results obtained using the two flows described above.

The Figure displays a window of an in-line section, located at 19,590 meters along the cross-line axis, and centered on the fault blocks where the data show numerous high-frequency diffractions. Figure 3a shows the section obtained by simple NMO and binning, while Figure 3b shows the results of AMO. As expected, the addition of AMO to the partial stacking process preserves the diffractions much better than simple NMO. Figure 3c shows the differences between the two sections; the diffractions are clearly evident. Figure 4 shows a similar comparison to that in Figure 3 but for the in-line location at 20,790. In this case also, the diffractions are better preserved by the addition of AMO. For both sections, AMO not only preserves the diffractions, but also decreases the amount of uncoherent noise. This effect is barely noticeable on paper plots, but it is quite evident on the computer screen. A possible explanation for this phenomenon is that the uncoherent stacking of the diffractions, and of other steeply dipping reflections, contributes to the general level of background noise in the data obtained by simple NMO-and-binning.

The next Figure (Figure 5) shows time slices cut at 1.068 seconds. As for the Figures above, Figure 5a shows the results of NMO and binning, while Figure 5b shows the results of AMO. The difference section (Figure 5c) clearly shows that few trends of high-frequency diffractions were not correctly preserved using the conventional process. The most evident differences tend to occur for reflections that are oriented at an angle with respect to the in-line direction. This observation is consistent with the fact that the conventional NMO-and-binning process is most inaccurate for reflection oriented at an angle of 45 degrees with respect to the nominal azimuth. Although there are not many of such reflections in this data set, which shows geological dips mostly aligned along the in-line directions, the AMO process enhances the ones that are present.

Figure 6 shows windows of an in-line section located at 20,940 meters and centered around the salt flank reflection visible in the lower-left corner of Figure 1. The dipping salt flank reflection is better preserved by the application of AMO. Further, as for the shallower section, also some midly dipping reflections appear to be “cleaner” after AMO.

CONCLUSIONS

The application of AMO to 3-D prestack data holds the promises to enable a considerable reduction in the computational cost of 3-D prestack depth imaging, without sacrificing the accuracy of the results.

The results presented in this paper show that the application of AMO improves the accuracy of partial stacking 3-D data over a range of offsets. In particular, the high-frequency steeply-dipping components of the reflected, or diffracted, energy benefit from the application of AMO. These components are crucial for the correct interpretation of complex fault systems, as well as for high-resolution imaging of complex reservoirs.

The next step in our testing procedure should be the application of a 3-D prestack depth migration method to the results of AMO, to fully analyze the advantages of including AMO in the 3-D prestack imaging flow.

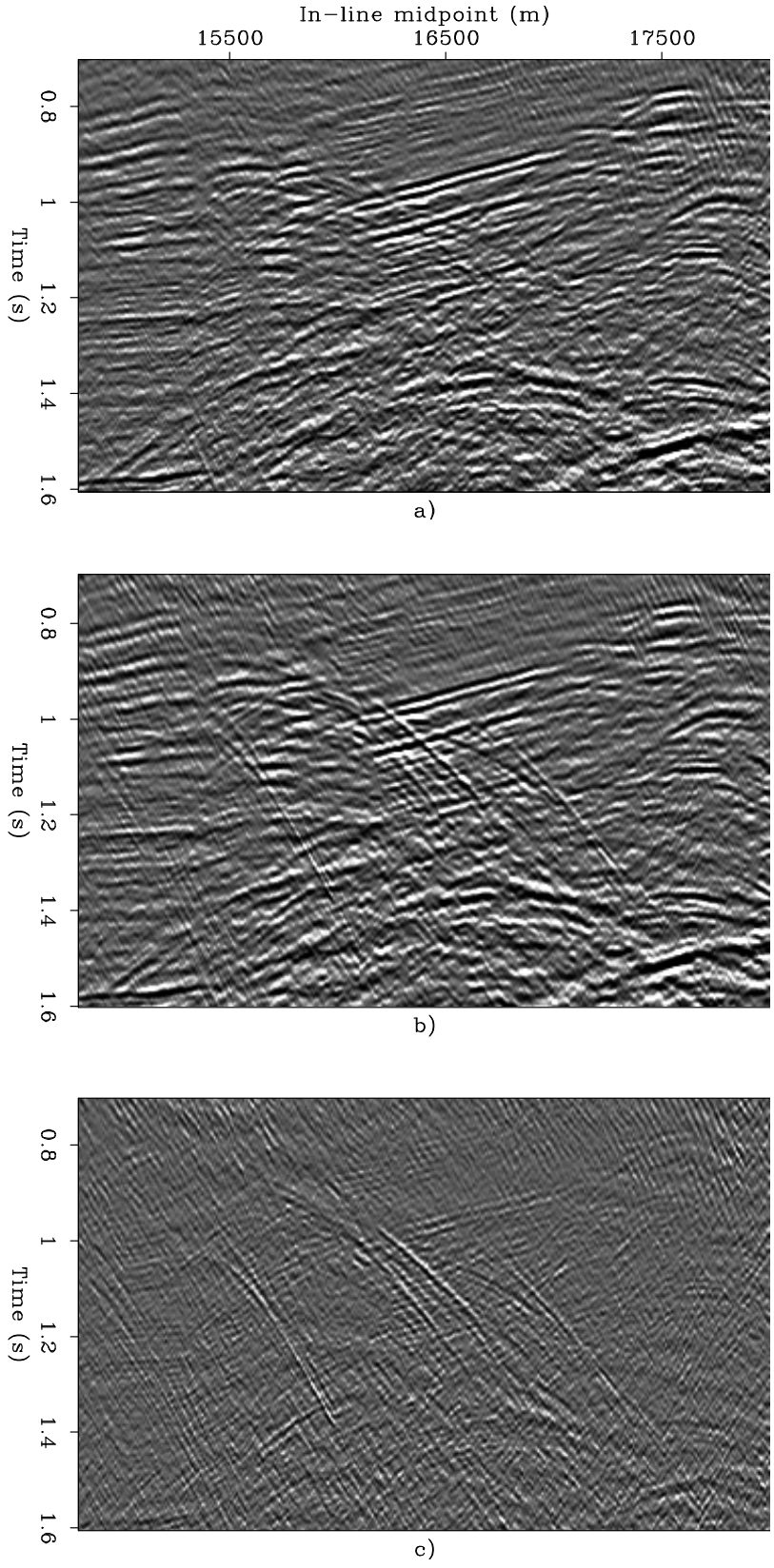

Figure 3: In-line sections (19,590 m) obtained by a) NMO-and-binning, b) NMO-and-AMO, c) subtracting a) from b) amo3d-Compup1 [NR]

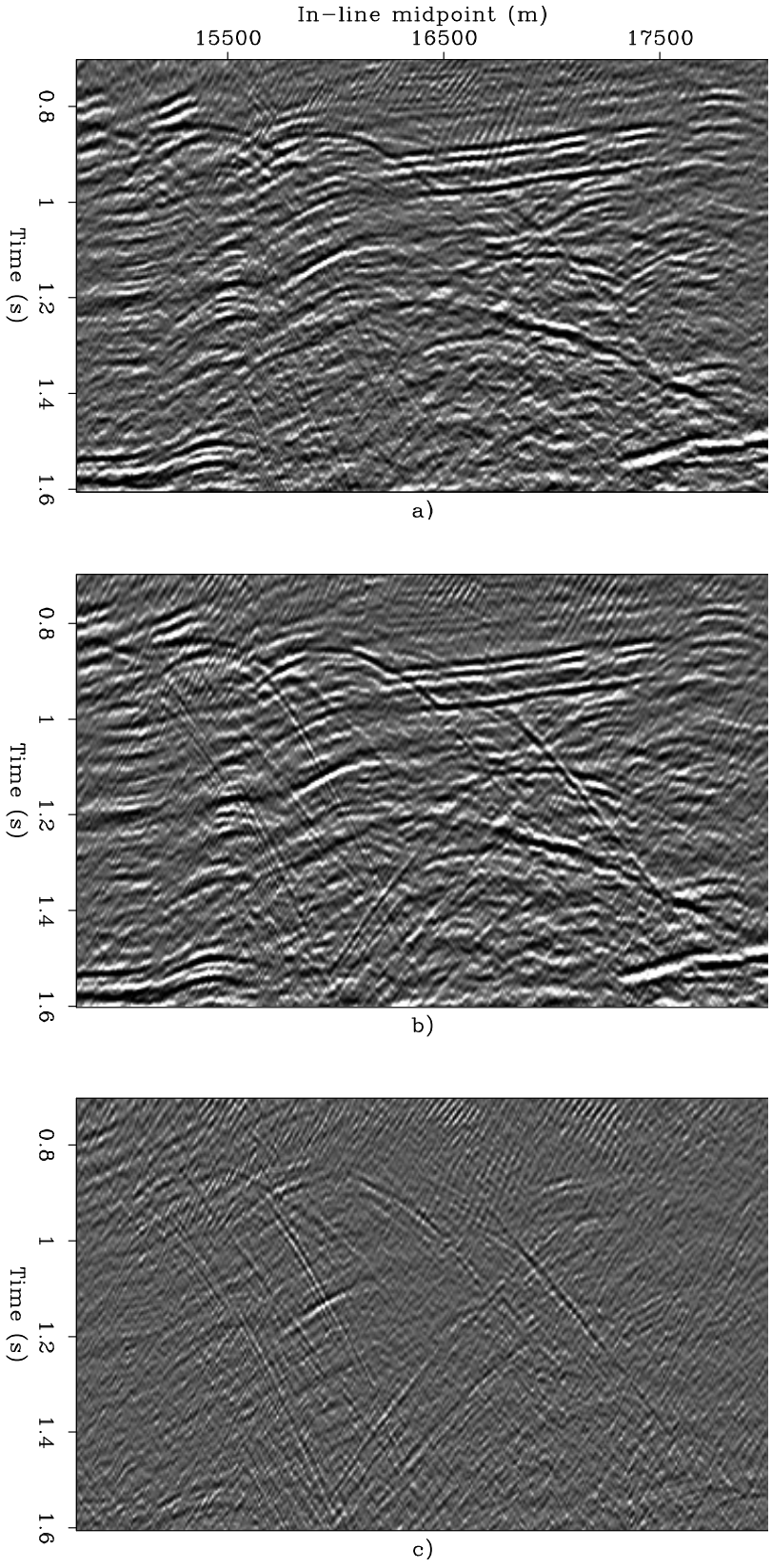

Figure 4: In-line sections (20,790 m) obtained by a) NMO-and-binning, b) NMO-and-AMO, c) subtracting a) from b) amo3d-Compup2 [NR]

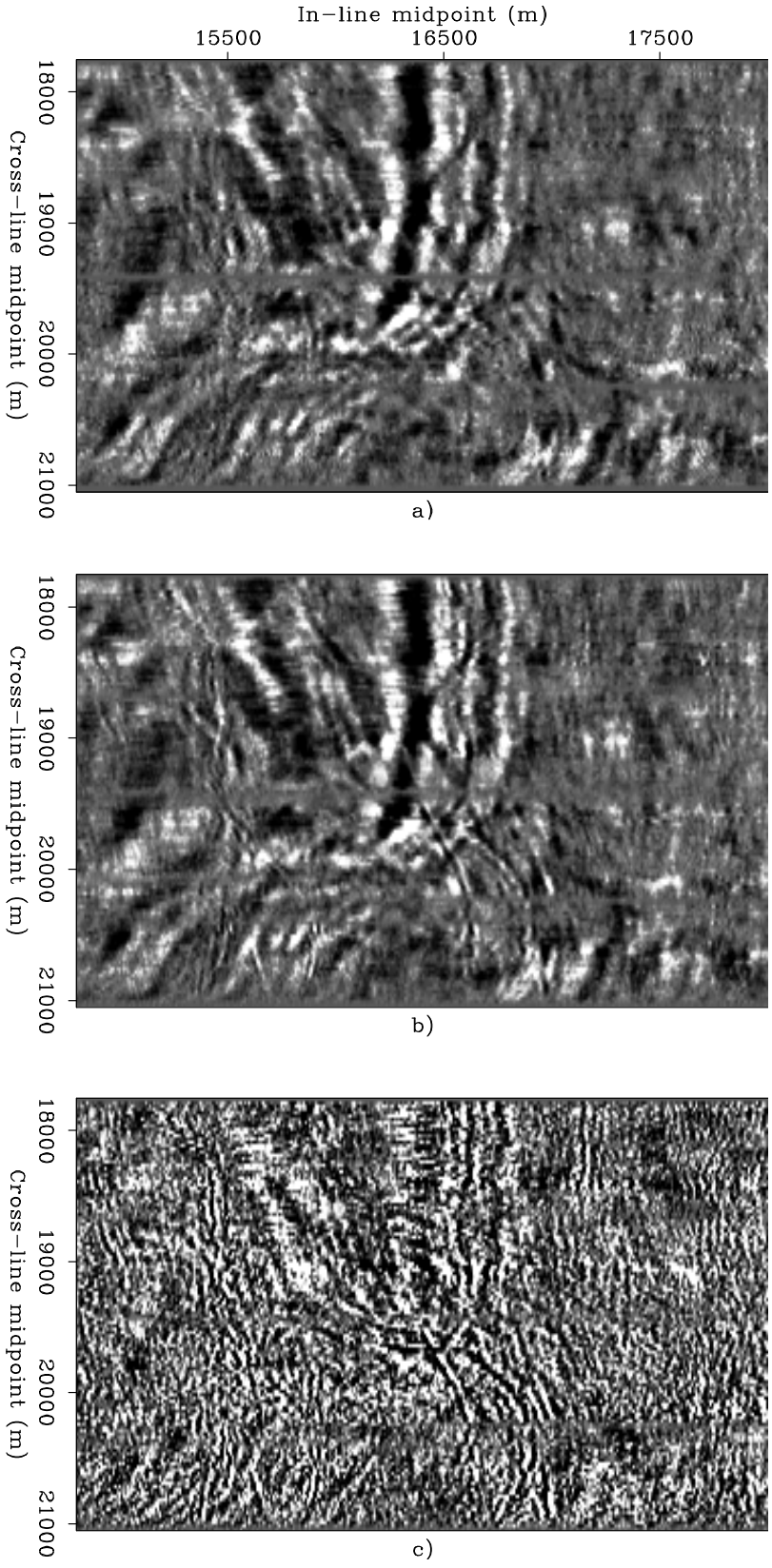

Figure 5: Time slices (1.068 s) obtained by a) NMO-and-binning, b) NMO-and-AMO, c) subtracting a) from b) amo3d-Compts [NR]

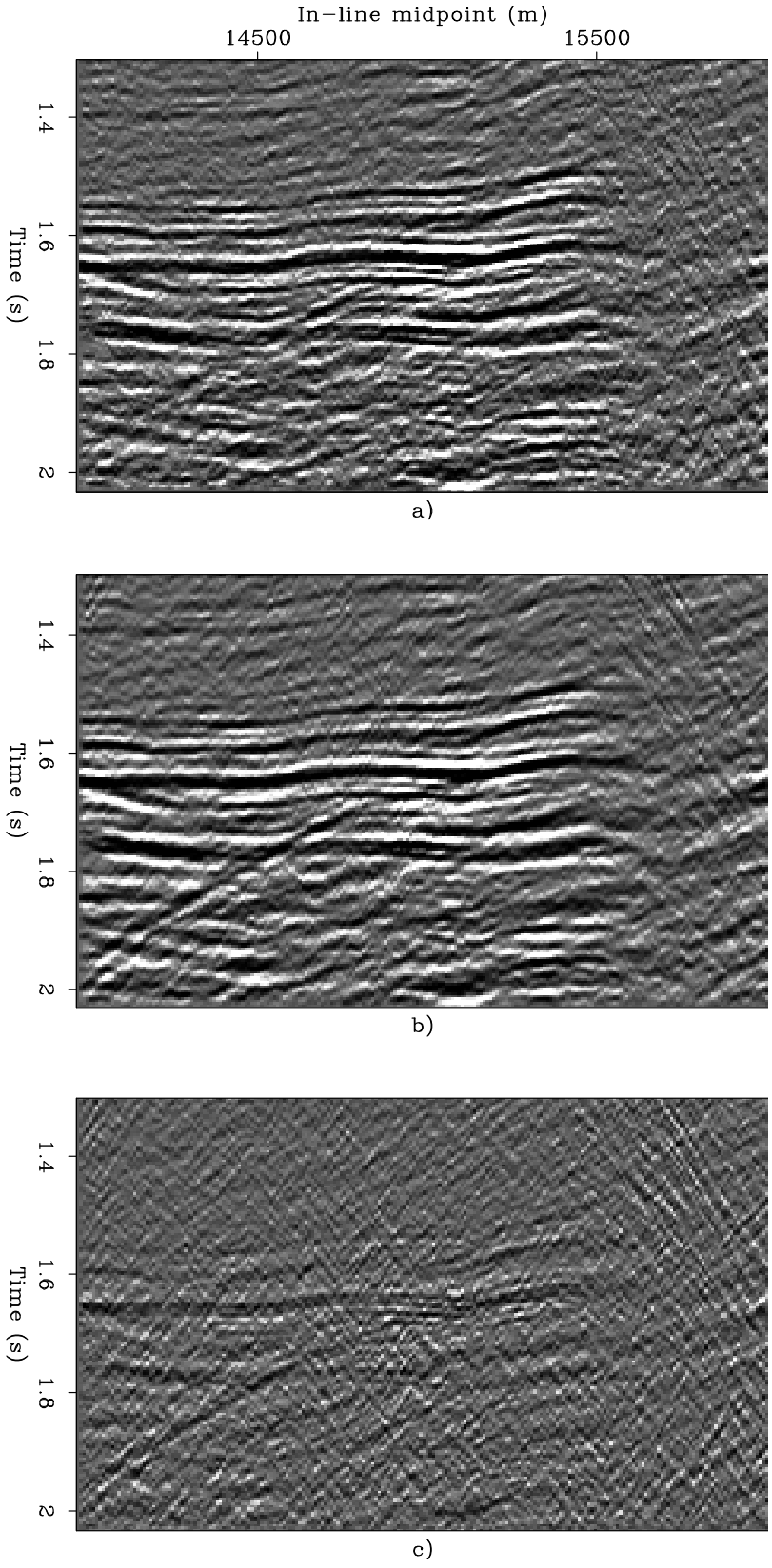

Figure 6: In-line sections (20,940 m) obtained by a) NMO-and-binning, b) NMO-and-AMO, c) subtracting a) from b) amo3d-Compll [NR]

ACKNOWLEDGMENTS

We would like to thank Conoco and its partners BP and Mobil, for agreeing to release the data to SEP. In particular, we would like to thank Doug Hanson of Conoco for giving us the opportunity to test our method on such an interesting data set, and for his successful efforts to actually send the data to us.

We would like to thank Silicon Graphics for loaning a 16-processors Power Challenge to SEP that has been the main computational platform for our tests.

The research presented in this paper was partially funded by the ACTI project # 4731U0015-3Q.

REFERENCES

Biondi, B., and Chemingui, N., 1994, Transformation of 3-D prestack data by Azimuth Moveout: SEP–**80**, 125–143.

Chemingui, N., and Biondi, B., 1995, Amplitude preserving AMO from true amplitude DMO and inverse DMO: SEP–**84**, 153–168.

Fomel, S., and Biondi, B., 1995a, The time and space formulation of azimuth moveout: SEP–**84**, 25–38.

Fomel, S., and Biondi, B. L., 1995b, Azimuth moveout: The operator parameterization and antialiasing: SEP–**89**, 89–108.

Fomel, S., 1995, Amplitude preserving offset continuation in theory Part 1: The offset continuation equation: SEP–**84**, 179–198.

Hanson, D. W., and Witney, S. A., 1995, 3-D prestack depth migration – velocity model building and case history: 1995 Spring Symposium of the Geophys. Soc. of Tulsa, Soc. Expl. Geophys., Seismic Depth Estimation, 27–52.

Zhou, C., and Schuster, G. T., 1995, Quasi-random migration of 3-d field data: 65th Ann. Internat. Mtg., Soc. Expl. Geophys., Expanded Abstracts, 1145–1148.

APPENDIX A

IMPLEMENTATION OF INTEGRAL AMO

In this Appendix, we describe the main characteristics of our implementation of the Kirchhoff AMO operator. This implementation is based on analysis presented in previous reports (Biondi and Chemingui, 1994; Chemingui and Biondi, 1995; Fomel and Biondi, 1995a,b). The AMO

integration surface has the shape of a saddle. The exact shape of the saddle depends on the azimuth rotation and offset continuation that are applied to the input data. When the azimuth rotation is small, the saddle has a strong curvature that makes its straightforward integral implementation inaccurate. We address this problem by performing the spatial integration in a transformed coordinate system. In this new coordinate system, the AMO surface is well behaved, and its shape is invariant with respect to the amount of azimuth rotation and offset continuation. The appropriate coordinate transformation is described by the following chain of transformations

$$\begin{bmatrix} z_1 \\ z_2 \end{bmatrix} = \begin{bmatrix} \frac{1}{|\mathbf{h_2}|\sin(\alpha_2-\alpha_1)} & 0 \\ 0 & \frac{1}{|\mathbf{h_1}|\sin(\alpha_2-\alpha_1)} \end{bmatrix} \begin{bmatrix} \cos\alpha_1 & -\sin\alpha_1 \\ \cos\alpha_2 & -\sin\alpha_2 \end{bmatrix} \begin{bmatrix} x_m \\ y_m \end{bmatrix}, \tag{A-1}$$

where x_m and y_m are the original midpoint coordinates, z_1, and z_2 are the transformed coordinates, and α_1 and α_2 are respectively the azimuth of the input trace and the azimuth of the output trace. The right matrix represents a space invariant rotational squeezing of the coordinate, while the left matrix is a simple rescaling of the axes by a factor dependent on the azimuth rotation $\alpha = \alpha_2 - \alpha_1$. When the azimuth rotation is zero, the transformation described in equation (A-1) becomes singular. In this case the AMO operator degenerates into the 2-D offset continuation operator (Biondi and Chemingui, 1994; Fomel, 1995). In practice, a simple pragmatic method to avoid the singularity is to set a lower limit for the product $|\mathbf{h_1}|\,|\mathbf{h_2}|\sin(\alpha)$. Since the 3-D AMO operator converges smoothly to the 2-D offset continuation operator (Fomel and Biondi, 1995a), the error introduced by this approximation is negligible. In this new coordinate system, the kinematics of AMO are described by the following simple relationship between the input time t_1 and the output time t_2.

$$t_2 = t_1 \sqrt{\frac{1-{z_2}^2}{1-{z_1}^2}}\,, \tag{A-2}$$

and the amplitudes (based on Zhang-Black amplitudes for DMO) are described by the following equation

$$A = t_2 \frac{\left(1+{z_2}^2\right)}{\left(1-{z_1}^2\right)\left(1-{z_2}^2\right)}\,. \tag{A-3}$$

Notice that this expression for the amplitudes does already take into account the Jacobian of the transformation described in (equation (A-1)). The result of the AMO integral needs also to be half-differentiated twice, once with a causal and once with an anti-causal differentiator.

Antialiasing

The AMO operator can be steeply dipping, and thus it is crucial to apply antialiasing to produce high-quality results. We apply antialiasing by a simple low-pass filtering of the input trace. The bandwidth of this low-pass filtering varies spatially along the operator and is a function of the local time dips of the operator. The time dips can be computed analytically

according to the following equations:

$$\frac{\partial t_2}{\partial z_1} = t_1 \frac{z_1}{1-{z_1}^2}\,, \tag{A-4}$$

$$\frac{\partial t_2}{\partial z_2} = t_1 \frac{z_2}{1-{z_2}^2}\,. \tag{A-5}$$

Operator aperture

The expression for the kinematic and amplitudes of AMO [equations ((A-2) and (A-3))] are valid for z_1 and z_2 ranging between -1 and 1. However, for finite propagation velocities, the AMO operator has much narrower aperture. Taking into account this finite aperture is crucial both for accuracy and for efficiency. For a given minimum propagation velocity V_{min}, the maximum output time can be evaluated according to the following expressions, as derived in (Fomel and Biondi, 1995a):

$$\gamma_1 = \frac{\frac{\partial t_2}{\partial z_1}}{|\mathbf{h_2}|\sin\alpha}\,, \tag{A-6}$$

$$\gamma_2 = \frac{\frac{\partial t_2}{\partial z_2}}{|\mathbf{h_1}|\sin\alpha}\,, \tag{A-7}$$

$$t_2 \le \frac{2}{V_{min}\sqrt{\left(\gamma_1^2+\gamma_2^2-2\gamma_1\gamma_2\cos\alpha\right)\left(1-{z_1}^2\right)}}\,. \tag{A-8}$$

To avoid truncation artifacts, we use a tapering function at the edges of the operator aperture.